



HAL
open science

MXene-supported single-atom and nano catalysts for effective gas-phase hydrogenation reactions

Yilong Yan, Djibril Sall, Lola Loupias, Stéphane Célrier, Mimoun Aouine, Pascal Bargiela, Mathieu Prévot, Franck Morfin, Laurent Piccolo

► **To cite this version:**

Yilong Yan, Djibril Sall, Lola Loupias, Stéphane Célrier, Mimoun Aouine, et al.. MXene-supported single-atom and nano catalysts for effective gas-phase hydrogenation reactions. *Materials Today Catalysis*, 2023, 2, pp.100010. 10.1016/j.mtcata.2023.100010 . hal-04284594

HAL Id: hal-04284594

<https://hal.science/hal-04284594>

Submitted on 14 Nov 2023

HAL is a multi-disciplinary open access archive for the deposit and dissemination of scientific research documents, whether they are published or not. The documents may come from teaching and research institutions in France or abroad, or from public or private research centers.

L'archive ouverte pluridisciplinaire **HAL**, est destinée au dépôt et à la diffusion de documents scientifiques de niveau recherche, publiés ou non, émanant des établissements d'enseignement et de recherche français ou étrangers, des laboratoires publics ou privés.



MXene-supported single-atom and nano catalysts for effective gas-phase hydrogenation reactions

Yilong Yan^a, Djibril Sall^a, Lola Loupias^b, Stéphane Célrier^b, Mimoun Aouine^a, Pascal Bargiela^a, Mathieu Prévot^a, Franck Morfin^a, Laurent Piccolo^{a,*}

^a Univ Lyon, Université Claude Bernard Lyon 1, CNRS, IRCELYON, F-69626 Villeurbanne, France

^b Université de Poitiers, CNRS, IC2MP, F-86073 Poitiers, France



ARTICLE INFO

Keywords:

MXene
 $Ti_3C_2T_x$
 Unstacking
 Single-atom catalyst
 CO_2 hydrogenation
 Butadiene hydrogenation

ABSTRACT

Transition metal carbides are known as efficient catalysts or catalyst supports and two-dimensional carbides (MXenes) offer renewed possibilities to anchor metal atoms and promote catalytic performances. This paper first presents an in-depth study of the elaboration of Pt or Pd-loaded $Ti_3C_2T_x$ MXenes and their unstacking for gas-phase catalysis investigations, along with step-by-step characterization by XRD, XPS, SEM and STEM. In particular, the influence of the MXene preparation method (HF vs. LiF-HCl etchants) on surface structure/composition and metal dispersion/oxidation state is disclosed. Second, the catalytic hydrogenation performances of these materials are reported, and reveal the interest of low-loaded Pt/MXene single-atom catalysts in terms of activity, selectivity and resistance to sintering. They present an unusually high selectivity to 2-butene – without butane formation – in butadiene hydrogenation, a model reaction of applied interest for the petrochemical industry. Moreover, in CO_2 reduction to CO (reverse water-gas shift reaction, relevant to greenhouse-gas valorization), these catalysts exhibit up to 99 % selectivity and a superior Pt-molar activity with respect to oxide-supported references. This work may stimulate the elaboration and investigation of other MXene-based systems for thermal heterogeneous catalysis, which remains rarely addressed on these materials.

1. Introduction

MXenes are recently discovered 2D materials, which generally behave as metallic conductors and exhibit promising properties in various fields such as (opto)electronics (e.g. electromagnetic shields and other components, antennas, conductive inks), energy conversion and storage (fuel cells, electrolyzers, batteries, supercapacitors), gas- and bio-sensors, and environmental remediation (carbon capture, water purification) [1–4]. MXenes are carbides, nitrides or carbonitrides of general formula $M_{n+1}X_nT_x$ where $n = 1-4$, M is an early transition metal (or a couple of them) such as Ti, V, Nb or Mo, X is C or/and N, and T_x are surface termination groups such as –O, –OH, –F, and –Cl. The latter depend on the synthesis protocol and more specifically on the acid etchant (s) when liquid-phase acid exfoliation – the most common route to date – is used to prepare a MXene from the corresponding MAX phase ($M_nA_{n+1}X_n$ layered 3D compound, where A is most often Al or Si) [5–7]. In the field of heterogeneous catalysis, the application of MXenes as electrocatalysts and photocatalysts, mostly for hydrogen production, has

been the object of massive interest. Comparatively, the thermocatalytic performances of MXenes [3,8], including hydrogenations, have been little investigated, which is most probably related to the inherent propensity of these 2D materials to stack under dry conditions, considerably reducing the accessibility of potentially active surface sites.

Notwithstanding, similar to classical transition metal carbides [9–11] (and other metal compounds), the surface of some MXenes exhibits late transition metal-like reactivity which provides them with intrinsic catalytic properties. Thus, Illas and coworkers have theoretically predicted the ability of MXenes to chemisorb CO_2 [12] and H_2 [13], making them good candidates for CO_2 capture [14] and conversion [15] through thermal hydrogenation [16,17] or electro/photo-reduction [18,19]. In the broad class of hydrogen-involving reactions such as hydrocarbon hydrogenation, dehydrogenation, reforming and water-gas shift, catalytic abilities have been revealed for $Ti_3C_2T_x$ (Ti_3CNT_x) [20–23], V_2CT_x [24,25], and Mo_2CT_x [26] MXenes.

However, compared to late transition metals, the surface reactivity of carbides and nitrides is often limited, e.g. regarding H_2 dissociation,

* Corresponding author.

E-mail address: laurent.piccolo@ircelyon.univ-lyon1.fr (L. Piccolo).

which stimulated a number of works aiming at promoting the reactivity of the first discovered and most studied MXene, $\text{Ti}_3\text{C}_2\text{T}_x$ [1], with late-transition-metal nanoparticles [27–33]. For example, Pt/ $\text{Ti}_3\text{C}_2\text{T}_x$ materials showed interesting performances in liquid-phase hydrogenation of nitroaromatics to amines [30]. Pt_3Ti and Pt_3Nb intermetallic nanoparticles were reported to form upon heating of Pt/ $\text{Ti}_3\text{C}_2\text{T}_x$ and Pt/ Nb_2CT_x under H_2 at up to 550 °C, and exhibited propane-to-propylene dehydrogenation properties with comparable performances between the two systems [27]. Besides, Pt nanolayers supported on $\text{Mo}_2\text{TiC}_2\text{T}_x$ were found active and stable for non-oxidative coupling of methane to ethane and ethylene [34].

Following the current wave of single-atom catalysis and related metal ultradispersion [35–38], several MXenes such as $\text{Ti}_3\text{C}_2\text{T}_x$ [39–45], Mo_2CT_x [46–49], $\text{Mo}_2\text{TiC}_2\text{T}_x$ [50], and V_2CT_x [51], were reported to anchor single metal atoms owing to the possibility of creating surface M vacancies [4,52–54]. In particular, Cu/ Mo_2CT_x was recently found efficient for CO_2 hydrogenation to methanol [49]. However, the thermochemical stability of atomic metal dispersion, which is a general issue in single-atom catalysis especially under reducing conditions [37], remains scarcely addressed on MXenes [55].

Herein, we first propose a methodology for the optimal preparation and conditioning of MXene-based samples for gas-phase catalysis. Three $\text{Ti}_3\text{C}_2\text{T}_x$ MXene samples, obtained via HF or LiF-HCl etching methods, were employed. Then, through a systematic study of Pt and Pd atomically dispersed on the MXenes, trends between the MXene surface state (depending on their preparation, storage and testing procedures), metal loading, single-atom stability and catalytic properties towards butadiene and CO_2 selective hydrogenations are established. The gas-phase hydrogenation of 1,3-butadiene to butenes is both of applied interest for polymerization/alkylation processes and a good model semi-hydrogenation reaction, that operates under mild T,P conditions and is usually catalyzed by palladium [56,57]. CO_2 hydrogenation to CO (reverse water-gas shift, RWGS), methane, methanol and other compounds of interest for greenhouse-gas utilization, is more demanding and is the subject of intense research, including on single-atom catalysts [58]. In this work, the excellent performance of the Pt/ $\text{Ti}_3\text{C}_2\text{T}_x$ system for RWGS, an important CO_2 valorization route for the energy transition [59,60], is revealed, together with the unusual selectivity of the single-atom catalyst in butadiene hydrogenation.

2. Materials and methods

The chemicals employed in this work, the preparation of reference catalysts, and the structural characterization and catalytic evaluation methods are described in [Supporting information](#).

2.1. MXene elaboration

A commercial $\text{Ti}_3\text{C}_2\text{T}_x$ MXene powder (referred to as CMX) was purchased from Easchem Co., Ltd. It was synthesized with the most usual method, implementing the (concentrated) HF etching protocol of a MAX phase. Homemade $\text{Ti}_3\text{C}_2\text{T}_x$ MXene (referred to as PMX, P standing for the University of Poitiers) was synthesized through a gentler alternative method which consists of *in situ* HF formation from LiF and HCl, based on the work of Benchakar et al. [7]. The Ti_3AlC_2 MAX phase precursor (0.5 g, initial particle size < 25 μm , see Ref. [7] for the MAX phase synthesis) was gradually added to LiF (0.8 g) dissolved in HCl (9 M, 10 mL). The reaction was run for 72 h at 60 °C under stirring. The suspension obtained after etching was centrifugated 8 times at 4500 rpm (corresponding to 2604 g – rotor F-34-6-38, Eppendorf centrifuge 5804) for 5 min and the supernatant liquid was systematically removed. These washing cycles are sufficient to reach a supernatant pH value higher than 5. The slurry was then filtered and dried overnight under air at room temperature (RT). As already proposed by one of us [61], the obtained MXenes were finally washed in deaerated water (350 mL) for 4 h to remove Al impurities by filtering

and drying at RT under air overnight. After filtration, a film is obtained, which reflects the formation of delaminated MXene.

2.2. MXene intercalation-delamination

For intercalation-delamination of CMX (leading to so-called int-CMX sample), we used the following protocol:

1. CMX (100 mg) was dispersed in dimethyl sulfoxide (DMSO, 10 mL) under magnetic stirring at RT for 24 h.
2. The resulting intercalant-CMX suspension was centrifugated at 3500 rpm for 5 min to separate the solid from the remaining liquid.
3. The powder was dried for subsequent characterization or put in deionized water for delamination (step 4).
4. After decanting the liquid (step 2), deionized water (20 mL) was added to int-CMX (100 mg) to wash and remove the intercalant in excess. Then the solution was sonicated (50 Hz) in an ice bath for one hour.
5. Finally, the delaminated CMX was recovered by centrifugation at 3500 rpm for 5 min, before characterization or metal impregnation.

For delamination of PMX, no intercalation step is required since Li^+ ions and water molecules are already inserted between the sheets during the etching step. A simple centrifugation step at 8500 rpm for 30 min was performed for recovering the delaminated MXenes in solid state.

2.3. Metal deposition on MXenes

Typically, delaminated $\text{Ti}_3\text{C}_2\text{T}_x$ (150 mg) was dispersed in deionized water (50 mL) and ultrasonicated for 15 min to form a suspension. Then, an aqueous solution (50 mL) containing a mother solution of H_2PtCl_6 (2 mL for 0.1 wt% metal loading or 20 mL for 1 wt%, 0.2 mg/mL) was slowly added dropwise to the MXene suspension at RT. After maturation for 8 h, the metal/ $\text{Ti}_3\text{C}_2\text{T}_x$ samples were collected and washed by centrifugation at 8500 rpm for 1 h with deionized water (100 mL) and dried in vacuum at 60 °C overnight. For Pd/MXene catalysts, the procedure was the same except that PdCl_2 (0.125 mg/mL) was used as metal precursor on PMX supports. For the two Pd/CMX catalysts, the water of the mother solution of PdCl_2 was replaced with an HCl solution (0.24 mol/L), in order to i) favor the deposition of metal species via the strong electrostatic adsorption (SEA) approach [62], and ii) increase PdCl_2 solubility [63], which facilitates the homogeneous distribution of Pd particles on the MXenes.

2.4. Unstacking of MXenes with solid oxides

The following materials were used for unstacking the metal/MXene catalysts for hydrogenation tests: Al_2O_3 (γ -phase, 99.997 % metal basis, 3 μm powder, 60 m^2/g , Alfa Aesar), TiO_2 (P25, 75 % anatase/25 % rutile, 50 m^2/g , Degussa), SiO_2 (Aerosil 200, amorphous, > 99.8 %, 200 m^2/g , Degussa), and quartz wool (QW, Helios Italquartz). Aerosil was calcined at 500 °C for 2 h in air [49], leading to a measured BET surface area of 214 m^2/g .

For drop casting on QW, the MXene (10 mg) was dispersed in distilled water (2 mL) under sonication for 5–10 min, to form a suspension. The latter was partially added dropwise on QW (50 mg), which was vacuum dried at 60 °C for 1 h. Then, another part of the suspension was added dropwise on the QW before a new drying. These steps were repeated until no suspension remained (around 4 times). Finally, the imbibed QW was vacuum dried at 60 °C overnight. For drop casting on alumina, the same procedure was used but the deposition was carried out in one go and with adapted quantities (10:40 mg and 50:350 mg of catalyst:alumina for butadiene and CO_2 hydrogenation, respectively).

For intercalation with titania and silica, the MXene (50 mg) was dispersed in distilled water (2 mL) under sonication for 15 min to form

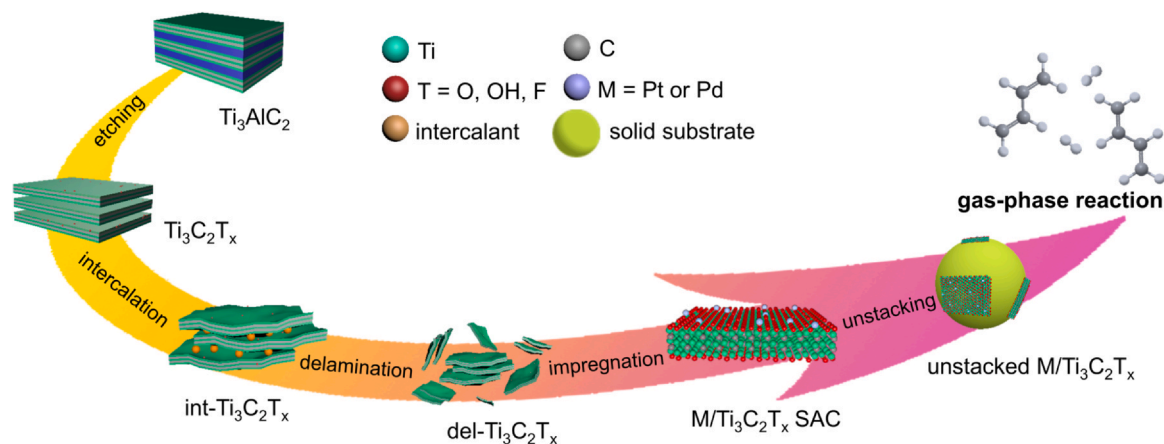


Fig. 1. Protocol for synthesis and application of metal/MXene catalysts in gas-phase reactions.

suspension A, and the oxide (350 mg) was dispersed in distilled water (2 mL) under sonication to form suspension B. A was slowly added into B, followed by sonication for 15 min and vacuum drying at 60 °C overnight.

2.5. Storage of MXene-based samples

To avoid oxidation, all the powder samples were stored in a glove box under argon or in a desiccator under primary vacuum. Before storage, the powders were dried at 60 °C under primary vacuum overnight to remove surface-adsorbed water as much as possible.

3. Results and discussion

3.1. Elaboration, delamination and impregnation of MXenes

One possible way to obtain a metal catalyst supported on a MXene for a gas-phase reaction is shown in Fig. 1. At least five stages can be identified, starting with the synthesis of the MXene by etching a MAX phase, followed by its intercalation, delamination, impregnation with a metallic precursor, and finally the “unstacking” of the 2D flakes of MXenes before carrying out the catalytic test. Each step of this protocol can influence the final catalytic activity. Intercalation, delamination and unstacking are specific steps required when MXenes – and more generally 2D stacked structures – are used as catalyst supports. Indeed, it is important to ensure that the largest possible MXene surface area is accessible i) to the metal precursors for deposition of the catalytic metal phase through extensive delamination, and ii) to the reagents in gaseous phase through e.g. drop casting on a solid oxide. The need for an optimal unstacking of the MXene sheets is well illustrated by the fact that the theoretical specific surface area of a single layer of $\text{Ti}_3\text{C}_2(\text{OH})_2$ MXene is 480 m^2/g [64], whereas N_2 adsorption volumetry, which provides a good quantification of the surface accessible to gaseous reactants, yields around 20 m^2/g for $\text{Ti}_3\text{C}_2\text{T}_x$ MXenes [65], or even less (14 m^2/g) [7]. This is consistent with the 19 m^2/g (BET) that we measured for the commercial HF-prepared $\text{Ti}_3\text{C}_2\text{T}_x$ MXene (CMX).

3.1.1. MXene elaboration

The MAX etching protocol greatly influences the final properties of $\text{Ti}_3\text{C}_2\text{T}_x$ MXenes in terms of morphology, nature of surface terminations, and type/amount of surface defects [5,7,66]. In the present study, $\text{Ti}_3\text{C}_2\text{T}_x$ MXenes synthesized via two distinct methods were considered. Commercial MXene (CMX) was obtained with the (“harsh”) original synthesis method [1] based on the HF etching protocol (details were not provided by the supplier), while a “softer” method was used to synthesize $\text{Ti}_3\text{C}_2\text{T}_x$ MXenes from LiF/HCl (PMX samples) [7,66]. However, within a given preparation method, the structure and the surface composition of the MXene can be subjected to subtle variations. In

particular, it is known that MXenes in colloidal solutions gradually oxidize in air or water [67,68], making the MXene structure and composition sensitive to storage/usage conditions and duration. Hence, we have compared two PMX samples, referred to as PMX1 and PMX2, prepared using the same “soft” method: while PMX1 was obtained via a controlled centrifugation/filtration/drying procedure followed by storage in inert atmosphere, PMX2 was exposed to ambient air in uncontrolled conditions leading to a higher degree of surface oxidation. This allowed us to investigate the influence of MXene oxidation on the properties of noble metal-based composites.

The morphology of the $\text{Ti}_3\text{C}_2\text{T}_x$ samples can be compared on the scanning electron microscopy (SEM) images of Fig. 2a,c,d and Fig. S1a,d,f. CMX reveals an accordion-like morphology as expected for high-concentration-HF-etching synthesis [5,7,64]. PMX samples exhibit a more compact, layered morphology, reflecting the typical microstructure of a delaminated MXene after restacking during the filtration step [7], without the large opening lamellas of CMX. The latter were attributed to the large and rapid evolution of H_2 during the exothermic reaction of HF with aluminum atoms of the MAX phase [5]. Compared to PMX1, PMX2 has a more defective, creased structure, which might be due to oxidation. PMX2 is also different from PMX1 at the macroscopic level, since PMX1 has a chewy and metal-like shiny texture whereas PMX2 is matte black, rigid, and brittle (Fig. 2c,d inserts).

Fig. 2f,g allows comparing the X-ray photoelectron spectroscopy (XPS) Ti 2p and C 1s core-level spectra of the three as-prepared MXenes. Figs. S2–S4 also show O 1s, F 1s and Cl 2p core-level spectra.

The Ti 2p_{3/2} level can be decomposed into four contributions [7]. The component at 455.0 eV corresponds to core titanium, surrounded only by carbon (C-Ti-C). The components at 455.8 ± 0.02 eV and 457.4 ± 0.04 eV, referred to as C-Ti²⁺-T_x and C-Ti³⁺-T_x, respectively, relate to surface titanium surrounded by carbon atoms and terminal groups (O, OH, F). Even if the assignment of the first three contributions is still much debated in the literature with many disagreements [7,69–72], they can be attributed without a doubt to Ti atoms of the MXene, unlike the last contribution at 459.4 ± 0.02 eV, which relates to an oxide or an oxifluoride phase, $\text{TiO}_{2-x}\text{F}_{2x}$. This fourth component reflects the level of MXene oxidation, which is negligible for PMX1, slightly more important for CMX, and extensive for PMX2 in accordance with the previous observation of its micro/macrostructure.

Generally, in the C 1s spectra, the component that originates from C atoms residing in Ti octahedra is centered at 281.9 eV in $\text{Ti}_3\text{C}_2\text{T}_x$ MXenes synthesized from fluorinated etching agents, and can therefore be used as an energy reference for the XPS spectra [69]. The other C 1s components can be attributed to contamination and – mostly – to amorphous carbon, which comes along with Ti oxidation [73]. Consistently, PMX1 appears poorer in amorphous C-C than CMX and – especially – PMX2, which is more oxidized.

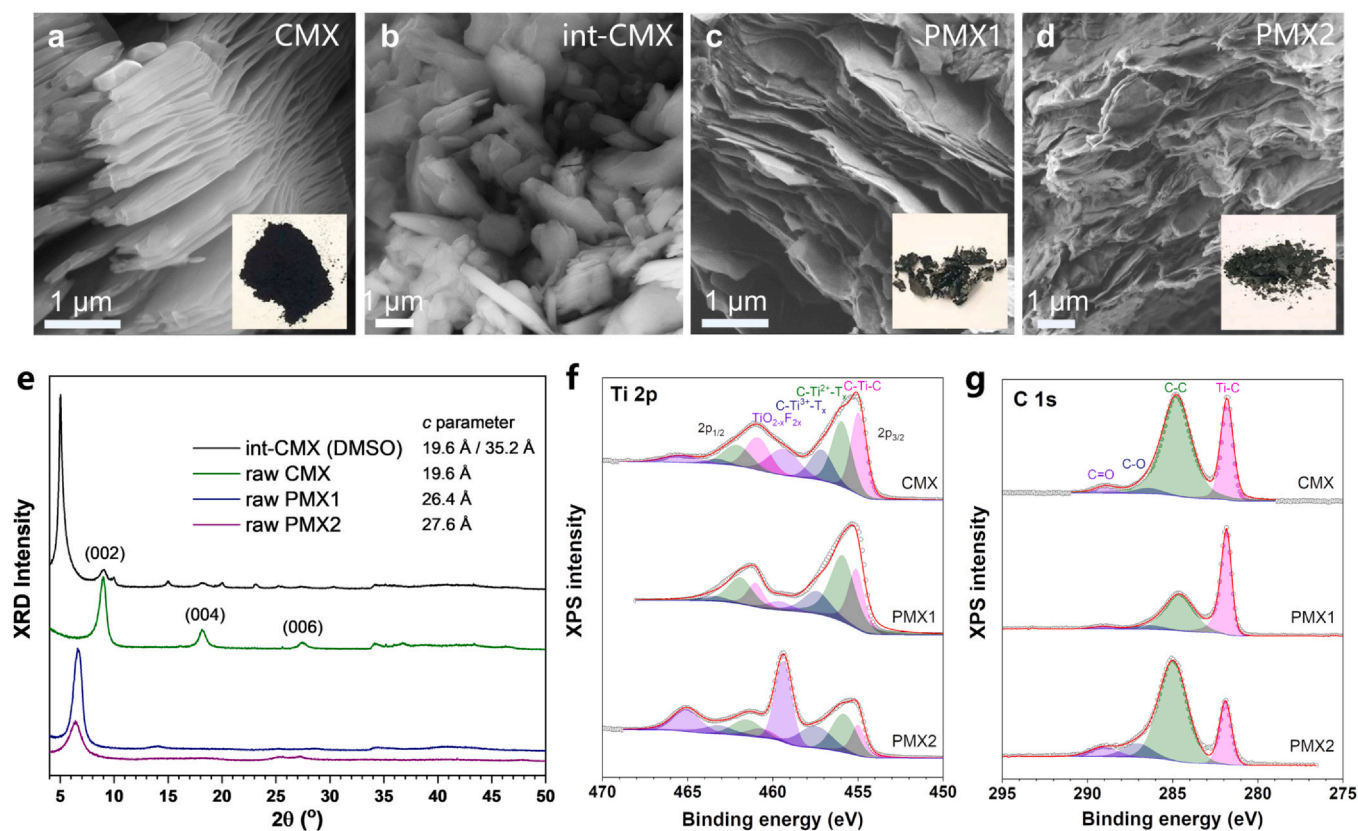


Fig. 2. MXene characterization. a–d) SEM images of as-prepared MXenes and CMX intercalated with DMSO (int-CMX). The inserts in a, c, and d show photographs (actual size *ca.* 5 cm) of the corresponding samples. e) XRD patterns of as-prepared MXenes and CMX intercalated with DMSO (the *c* parameter of the crystallographic unit cell is indicated). f, g) Ti 2p and C 1s XPS spectra of as-prepared MXenes.

The O 1s spectral region can result from many contributions (terminal groups, oxides, impurities, water), leading to contradictions in the literature. Hence, we focus on the component at 530.7 eV, which is well documented to originate from titanium oxyfluoride [7,69]. Consistently with Ti 2p $\text{TiO}_{2-x}\text{F}_{2x}$ component and C 1s C-C component, the O 1s $\text{TiO}_{2-x}\text{F}_{2x}$ component area varies in the order: $\text{PMX1} < \text{CMX} < \text{PMX2}$.

The total amount of fluorine at the MXene surface, as measured by XPS, ranges between 6 at% (PMX2) and 16 at% (CMX), as reported in Fig. S5d. The total amount of chlorine is 3–4 at% on PMX samples according to XPS and X-ray fluorescence (XRF) analyses. CMX-based samples do not show any Cl signal from XPS or XRF, which suggests that residual Cl on PMX samples originates mainly from LiF-HCl etching, not from metal precursors. Halogens (F, Cl...) are likely to influence surface properties such as metal electronic structure and catalytic performance [74]. However, without proper control of their concentration (which is beyond our scope herein), their effect can hardly be identified. The amount of lithium, which could not be determined by XPS, was measured to be only 0.39 wt% in PMX1 and 0.34 wt% in PMX2 by inductively coupled plasma-optical emission spectroscopy (ICP-OES).

3.1.2. Intercalation-delamination

Delamination of MXenes often requires the weakening of the interactions between the 2D sheets [75]. This key step is necessary for MXenes synthesized by HF etching (CMX) and is frequently achieved by intercalating an organic compound. In a preliminary study, we tested a number of intercalants (urea, ethylene glycol, tetramethylammonium hydroxide, DMSO), and as a result we kept DMSO as the most efficient one (SI, Experimental section and Fig. S6a,b). In contrast, when using lithium-containing etchants such as the LiF-HCl solution (PMX), the

solvated Li^+ ions act as the intercalant, and no subsequent intercalation is required [5].

For intercalation-delamination of CMX, the MXene powder was dispersed in DMSO, centrifuged, washed, then sonicated in iced water (in order to prevent oxidation of the MXenes near RT) [76], and finally recovered by centrifugation (see Section 2.2 for details). The effect of the sonication time (1–10 h) on X-ray diffraction (XRD) structure was investigated. The shortest duration (1 h) was retained since it led to the highest interlayer distance while limiting the experimental time and thereby the MXene degradation (SI, Experimental section and Fig. S6c).

The XRD patterns of as-prepared CMX, intercalated CMX (int-CMX), and as-prepared PMX samples are shown in Fig. 2e. The (002) diffraction line angular positions for PMX samples are lower than that for CMX, indicating that the interlayer spacing of PMX ($c = 26.4\text{--}27.6 \text{ \AA}$) is larger than that of CMX ($c = 19.6 \text{ \AA}$). This is consistent with the insertion of water layers stabilized with Li^+ cations in the case of PMX samples [77]. The significant variation commonly observed for *c* (e.g. between 26.4 and 27.6 Å herein) and the asymmetry of (002) lines reflect that an interstratification process is at stake in these materials (as in clays). It corresponds to a random distribution of interlayer spacings due to the presence of one or two water layer(s) in the same crystal [77]. Besides, DMSO intercalation in CMX leads to a significant increase in the *c* parameter, from 19.6 to 35.2 Å. However, int-CMX still shows a small (002) peak at the initial value of 9.0° , which means that a small fraction of CMX was not intercalated.

After intercalation, the accordion-like/lamellar morphology of CMX is replaced with a more disordered morphology (Fig. 2b). This means that during the recovery of the powder, the flakes restacked randomly. However, a few small stacks of ordered nanosheets (giving rise to the (00l) diffraction peaks) can be seen (Fig. S1b). This suggests that some nanosheets regained their ordered stacking during the centrifugation

step, or – more probably – were not completely delaminated. As a matter of fact, when MXene sheets are delaminated, the restacking observed in recovered powders or films is mostly random, without structural order [7].

3.1.3. Metal deposition

Following the work by Zhao's group [39], for the vast majority of catalysts, Pt and Pd were deposited onto the delaminated MXenes using the traditional wet-impregnation method, which consists in contacting the powders with an aqueous solution of metal salt precursors. According to the authors, the metal cations can be reduced by Ti vacancy defects at the MXene surface without any additional reducing agent or heat treatment. They also report that these sites are ideal for accommodating and stabilizing single metal atoms [39]. The delaminated MXene was suspended in water and a solution of the metal precursor was added dropwise; after maturation, centrifugation, and drying, the solid catalysts were obtained (see details in Section 2.3). To promote PdCl₂ solubility and Pd deposition by SEA [62], hydrochloric acid was added for the preparation of the two Pd/CMX catalysts. The addition of HCl favors the speciation of Pd species to the anionic PdCl₄²⁻ complex [78] and lowers the pH under the point of zero charge (PZC) of the Ti₃C₂T_x surface, which was measured at pH 2.7 by Shahzad et al. [79]. Thus, the MXene surface was positively charged and available for the anionic Pd-complex adsorption.

3.2. Characterization of metal/MXene catalysts

Table 1 lists the main characteristics of all the synthesized catalysts. The samples are denoted xM/CMX or xM/PMX_n, where x is the target loading (0.1 or 1 wt%), M the deposited metal (Pt or Pd), and n the number of the PMX batch (1 or 2).

3.2.1. Metal content and dispersion

Annular dark-field scanning transmission electron microscopy (ADF-STEM) imaging was used to evaluate the relative abilities of the MXenes to immobilize single metal atoms. Fig. 3a–d shows representative images for PMX1, while their counterparts for PMX2 and CMX are reported in Fig. S7. At low metal loading (0.1 wt%), both PMX samples stabilize Pt and Pd single atoms, whereas on CMX, minority Pt clusters (size < 2 nm) or majority fcc Pd NPs (5 nm in size) were also detected. At higher loading (1 wt%), all Pt/MXene samples show a mixture of single atoms and clusters/small NPs. Mostly NPs (4–9 nm) or even larger aggregates are visible on 1 wt% Pd catalysts.

Table 1

Characteristics of the MXene-supported Pt and Pd catalysts.

Catalyst ^a	Precursor	Loading [wt%] ^b	Metal species ^c
0.1Pt/PMX1	H ₂ PtCl ₆	0.12	SAs ^d
0.1Pt/PMX2	H ₂ PtCl ₆	0.10	SAs
0.1Pt/CMX	H ₂ PtCl ₆	0.15	SAs and clusters
1Pt/PMX1	H ₂ PtCl ₆	0.92	SAs and NPs (2.3 ± 0.8 nm)
1Pt/PMX2	H ₂ PtCl ₆	0.37	SAs, clusters and NPs
1Pt/CMX	H ₂ PtCl ₆	0.82	SAs and clusters
0.1Pd/PMX1	PdCl ₂	0.09	SAs (unstable in reaction)
0.1Pd/PMX2	PdCl ₂	0.06	SAs
0.1Pd/CMX	PdCl ₂ /HCl	0.13	NPs (5.0 ± 0.8 nm)
1Pd/PMX1	PdCl ₂	0.80	NPs (3.9 ± 1.2 nm) and aggregates
1Pd/PMX2	PdCl ₂	0.58	SAs and aggregates
1Pd/CMX	PdCl ₂ /HCl	0.41	NPs (9.1 ± 2.6 nm)

^a The first number denotes the target metal loading in wt%.

^b Pt or Pd loading determined from ICP-OES.

^c Determined from ADF-STEM.

^d "SAs" and "NPs" correspond to single atoms and nanoparticles, respectively.

It is worth noting that the target loading of 1 wt% was hardly reached in most cases, with measured values of 0.37, 0.58 and 0.41 wt % for 1Pt/PMX2, 1Pd/PMX2 and 1Pd/CMX, respectively, even when the SEA approach was used. In contrast, the metal loadings are close to the expected value for PMX1 samples, i.e. 0.92 wt% for 1Pt/PMX1 and 0.80 wt% for 1Pd/PMX1 (Table 1). This suggests a relatively low density of anchoring sites (such as Ti vacancies) [39] at the MXene surfaces together with a lower extent of delamination for PMX2 and CMX samples compared to PMX1. Indeed, delamination of oxidized MXenes is likely to be inhibited by the oxides, which may form connecting bridges between the sheets. These limitations are consistent with the tendency to form clusters/NPs (and even aggregates for Pd) on MXenes at high metal loading.

3.2.2. Bulk structure and texture

The XRD patterns of all the samples are shown in Fig. S8, while the data for PMX1 samples are reported in Fig. 3e. For both PMXs, some variations in the positions of the (002) peaks are observed, but they are not large enough to conclude on possible metal insertion between the layers, since they could originate from interstratification [77].

For PMX1-based samples, the (002) peak disappears for high-loading catalysts, which may occur for two reasons: i) full delamination may result in a highly disordered arrangement of MXene sheets during the drying-recovery step [80]; ii) extensive oxidation of the MXene may lead to structural collapse [81]. The layered morphology of the metal/PMX1 catalyst visible on the SEM image in Fig. 3a (insert), as well as the presence of titania crystallites identified from diffractograms of Fig. 3e, favor the latter hypothesis. However, this phenomenon is not observed for PMX2 samples, although they are more oxidized, according to the anatase and rutile TiO₂ diffraction peaks present in all the diffractograms – except the raw MXene for rutile (Fig. S8b). Moreover, SEM images of Pt/PMX2 samples show small titania crystals (Fig. S1g,h). Due to its initial oxidized state, PMX2 is less delaminated than PMX1, hence part of the MXene may not be in contact with the oxidizing environment during the metal deposition procedure, explaining why the (002) peak is retained. This result thus supports a lower state of delamination for PMX2.

For CMX, the (002) diffraction line, which had moved to 2θ = 5° after DMSO intercalation (Fig. 2e), moves back to 9° after metal deposition, whatever the metal nature and loading (Fig. S8c). This value, which corresponds to that of the non-intercalated raw CMX, is likely due to the full loss of the DMSO intercalants upon metal deposition in water. Moreover, like for PMX2, the (002) peak remains whatever the metal loading, suggesting again a low delamination degree for this sample.

3.2.3. Surface chemistry

Fig. 3f,g shows XPS spectra for Ti 2p and C 1s core levels in PMX1-based samples, while Figs. S2–S5 reports all the XPS data. For all the MXenes, the amounts of TiO_{2-x}F_{2x} phase and amorphous carbon (C-C) increase together with the metal loading, and Pd-containing samples are systematically richer in C-C than Pt-containing ones. This makes sense when one considers that Ti oxidation scales with C-C formation (as previously discussed, and essentially validated in Fig. S5e for the whole sample series) and metal reduction. As a matter of fact, the deposition of metals leads to significant oxidation of the MXenes (Ti⁴⁺ formation), which increases with the metal loading, and is greater for Pd samples. This is consistent with surface Ti oxidation increasing with the number of deposited metal atoms (which is about twice for Pd compared to Pt at similar weight loading), regardless of the metal nature.

The Pt 4f and the Pd 3d spectra of high-loading (1 wt% metal) catalysts are reported in Fig. 4. Note that the Pt 4f signal overlaps with an Al 2p contribution owing to the presence of Al-containing impurities in MXenes (0.11, 0.03 and 2.13 wt% Al in PMX1, PMX2, and CMX, respectively, as determined from ICP-OES). They can be in the form of

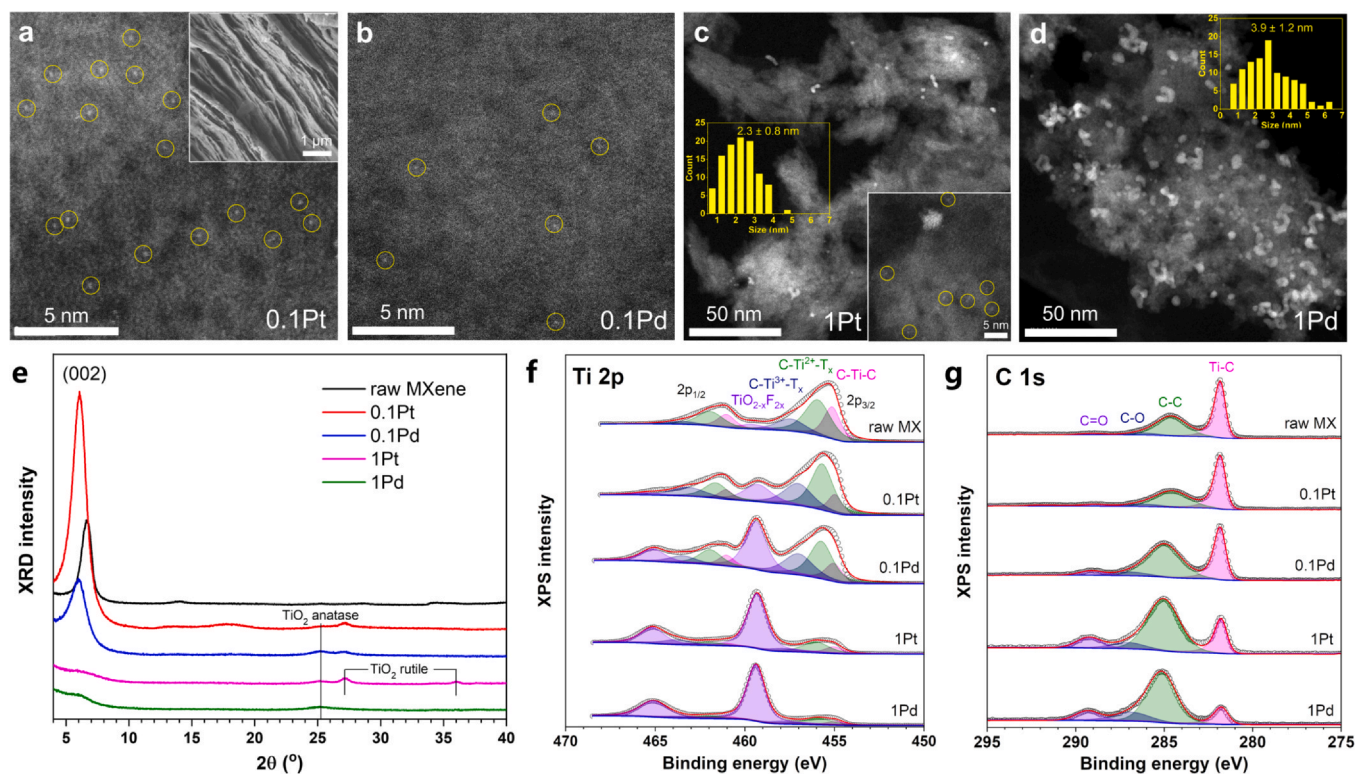


Fig. 3. Metal/MXene catalyst characterization. ADF-STEM images (a–d), XRD patterns (e), Ti 2p XPS spectra (f), and C 1s XPS spectra (g) of PMX1-based samples. The insert in a is a SEM image of 0.1Pt/PMX1.

residual non-etched Ti_3AlC_2 (MAX) crystallites, AlF_x species, or/and alumina particles; the position of the Al 2p contribution suggests that the main Al impurities are AlF_x in the PMX samples and alumina in CMX [82,83].

These results confirm that a simple impregnation at RT, without any other treatment, is sufficient to reduce and stabilize metal atoms [39] on the three $\text{Ti}_3\text{C}_2\text{T}_x$ MXenes samples. Besides, MXene oxidation is not balanced by metal reduction, *i.e.* Ti oxidation extent is much more important when one accounts for the molar $\text{TiO}_2/\text{Pt(Pd)}$ ratio, which suggests that metal deposition catalyzes the oxidation of MXenes in the presence of water and/or dissolved oxygen. In addition, the self-reduction process is more efficient for Pd, which is reduced into the metallic state in a significant proportion, than for Pt which is largely in oxidation state II and higher. This can be related to the fact that Pd is in oxidation state II in the used precursor, while Pt is IV, implying that fewer electrons are needed to reduce Pd.

Finally, the oxidation states of Pt and Pd vary in opposite ways with the supports: Pd is more reduced on CMX while Pt is more reduced on PMX1, and PMX2 is intermediate. Notably, the most reduced metal species roughly correspond to the least dispersed ones (1Pd/CMX and 1Pt/PMX1), while the more oxidized metals correspond to the most dispersed ones (in particular for 1Pt/CMX, which is atomically dispersed). Thus, it can be assumed that the oxidized metal fraction corresponds to SAs stabilized at surface vacancies and other defects, and that the metallic fraction, which is more mobile, is rather in the form of nanoparticles or clusters.

3.3. Catalyst unstacking and hydrogenation performances

3.3.1. Unstacking

As the $\text{Ti}_3\text{C}_2\text{T}_x$ MXenes were largely re-stacked after impregnation and drying-recovery, an unstacking step was used to delaminate again the MXenes up to the potential formation of single layers, which would allow the reactant gases to access as many active sites as possible. Two strategies were developed. The first one used the metal/MXene

catalysts as inks to drop cast onto micrometric solid substrates such as quartz wool (QW) and $\gamma\text{-Al}_2\text{O}_3$. The second strategy consisted in the intercalation of particles of a nanometric powder such as TiO_2 (P25) or SiO_2 (Aerosil 200) between metal/MXenes sheets to keep interlayers open, using a procedure resembling the drop-casting method employed for QW and alumina (see Section 2.4).

Fig. 5 shows representative SEM images of Pt/MXene materials dispersed on the oxides. After deposition, the morphology of MXenes was changed according to the different structures of these oxides. In the case of drop casting (a,b), both substrates are partially coated with MXene flakes, including multilayers (insert). In the case of solid intercalation (c,d), the MXenes are partially covered with TiO_2 or SiO_2 particles. As discussed below, after comparisons, quartz wool and silica nanopowder were selected for butadiene and CO_2 hydrogenation tests, respectively. The pure oxides were checked to be inactive for these reactions (conversion < 1% in the whole temperature ranges).

3.3.2. Butadiene hydrogenation

Fig. S9a compares the catalytic activity in 1,3-butadiene hydrogenation of the 0.1Pd/PMX1 catalyst drop casted on QW or alumina, with that of a mechanical mixture of alumina and the pure as-prepared (non-unstacked) catalyst, and that of the pure catalyst. The reaction was performed in a gas-phase flow reactor, at atmospheric pressure, between RT and 200 °C (SI, Experimental section). Owing to the increase in catalyst surface area, the activity measured on the unstacked catalysts is higher. Moreover, drop casting on QW provides better results than on alumina. QW was thus selected for the following butadiene hydrogenation tests.

The full series of metal/MXene catalysts, as well as bare MXenes, Pt/ Al_2O_3 and Pd/ Al_2O_3 nanocatalyst references (TEM/STEM images in Fig. S10a,b), were compared. The samples were pretreated for 1 h at 400 °C in H_2 flow, which appeared optimal with respect to 240 °C, 600 °C or no pretreatment (Fig. S9b). The noble metal-free MXenes were found slightly active, in the order: CMX < PMX2 < PMX1 (Fig. S9c). The conversion vs. temperature results for Pt and Pd series are presented in

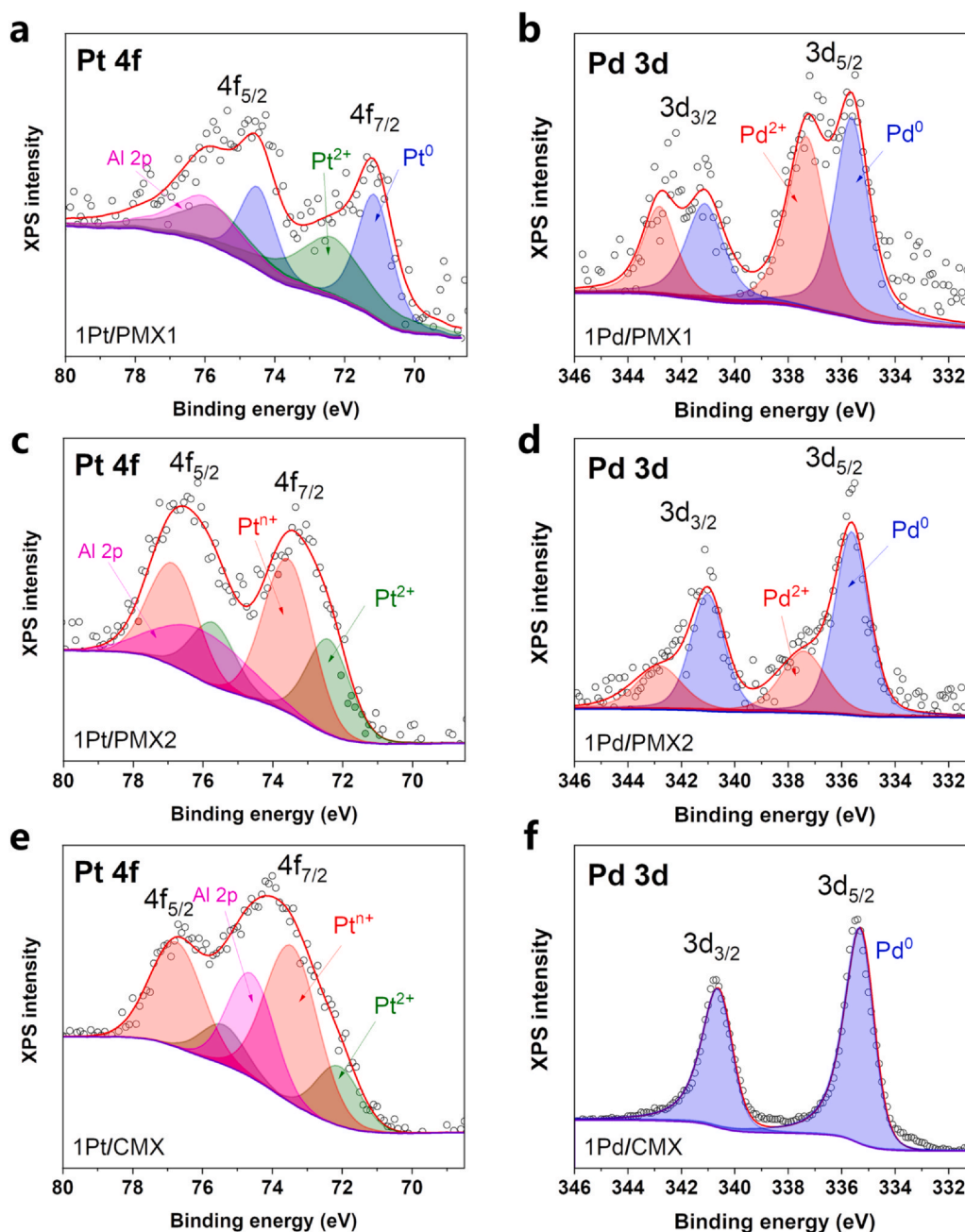


Fig. 4. XPS characterization of supported metals. Pt 4f (left column) and Pd 3d (right column) XPS spectra and numerical fitting for 1 wt% metal on PMX1 (a, b), PMX2 (c, d), and CMX (e, f). Pt 4f overlaps with Al 2p contribution.

Fig. S11a,b, the corresponding Arrhenius plots are shown in Fig. S11c,d, and the product distributions (selectivities) at iso-conversion are reported in Fig. S12. The results from the data recorded at 50 °C are summarized in Fig. 6a, where the catalysts are ranked by molar activity.

General trends can be found. First, Pd-based catalysts are generally more active and more selective to butenes than Pt-based ones, as expected from the literature on metal surfaces and nanoparticles [84–86]. In contrast, Pd catalysts are less stable than Pt ones, as can be seen from the difference between the heating run and the cooling run, as well as the saturation in conversion for several Pd catalysts (Fig. S11a,b). Consistently, conventional Pd catalysts are known to promote alkene oligomerization (“green oil”), leading to deactivation [56,87]. Fig. S13 reports isothermal reaction tests of Pt/PMX1 samples for 12–24 h on stream, showing that significant activity is retained at this timescale, without major change in selectivity.

Overall, the most active MXene-supported catalysts are the two Pd/PMX1 ones, but they are less active than Pd/Al₂O₃ with similar selectivity. Actually, the most remarkable system is 0.1Pt/PMX1 (and to a lower extent, 0.1Pt/PMX2) as it exhibits a specific selectivity, with a high fraction of 2-butenes (62% at 50 °C) while showing no butane production and a relatively high molar activity (0.25 s⁻¹ at 50 °C). This product distribution is substantially different from that obtained for Pt/Al₂O₃, which, at comparable conversion, expectedly [84–87] presents a lower selectivity to butenes (corresponding to 15% butane at 50 °C), and a high selectivity to 1-butene (59% at 50 °C) like Pd/Al₂O₃. 1Pt/MXene catalysts also are leading to butane formation. Notably, 0.1Pt/PMX1 and 0.1Pt/PMX2, which are the most selective to 2-butenes, also show the lowest apparent activation energy of the Pt series (25–27 kJ/mol vs. 32–54 kJ/mol, Fig. S11c). Besides, post-reaction STEM analyses (Fig. S14) show that the single-atomic dispersion of platinum in 0.1Pt

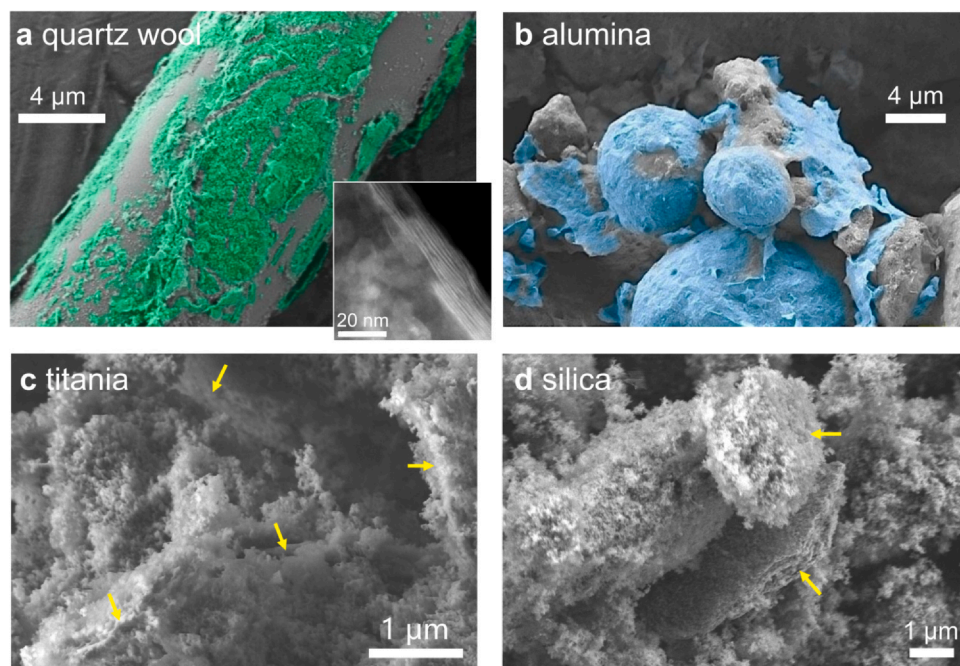


Fig. 5. SEM characterization of unstacked catalysts. SEM images of 0.1Pt/PMX1 (a, b) and 0.1Pt/PMX2 (c, d) unstacked with several oxides. The insert in a is an ADF-STEM image of MXene multilayers (0.1Pt/PMX2) deposited on quartz wool. Green and blue colors in a and b indicate MXene sheets or flakes. Arrows in c and d point to MXene flakes.

samples is essentially retained, whereas the high-loaded Pt/PMX samples are not SACs. Put together, these observations point to a SAC-specific reaction mechanism for Pt/PMX.

XPS analyses were carried out on selected catalysts after testing in butadiene hydrogenation. After the H_2 pretreatment and the reaction run, the MXenes are slightly reduced (Fig. S5, decrease of $TiO_{2-x}F_{2x}$ fraction), suggesting the partial reduction of titania impurities. On the three MXenes, the F 1s core-level spectra show a component centered at 688–689 eV after reaction, which is also present before reaction for PMX2-supported catalysts only (Figs. S2–S4). In general, the F 1s spectrum of MXenes elaborated with fluorinated compounds presents two components. The strongest one, located around 685 eV, is attributed to surface terminations of the C-Ti-F type and the second one, which is weaker and located at 686–687 eV, is assigned to a set of species, often called "F impurities" [69,70], that mainly include AlF_x

species [82,88]. The high-energy component is rarely reported in the MXene literature but it could be attributed to organic fluorinated species ($-CF_x$ species) [7,82]. A fraction of the amorphous carbon (that comes along with Ti oxidation, notably for PMX2 before reaction) and part of the oligomers formed in the course of butadiene hydrogenation [56,87] (all samples) may be fluorinated by the F atoms initially present as C-Ti-F or $TiO_{2-x}F_{2x}$ species. Finally, it must be mentioned that this high-energy component was previously attributed to fluorine contained in a nonstoichiometric $TiO_{2-x}F_x$ solid solution formed during the preparation of an F-doped TiO_2 material [89].

3.3.3. CO_2 hydrogenation

The RWGS reaction ($CO_2 + H_2 \rightarrow CO + H_2O$), an important route of CO_2 valorization, is endothermic and in competition with other pathways such as methane and methanol formation [90]. Thus, achieving

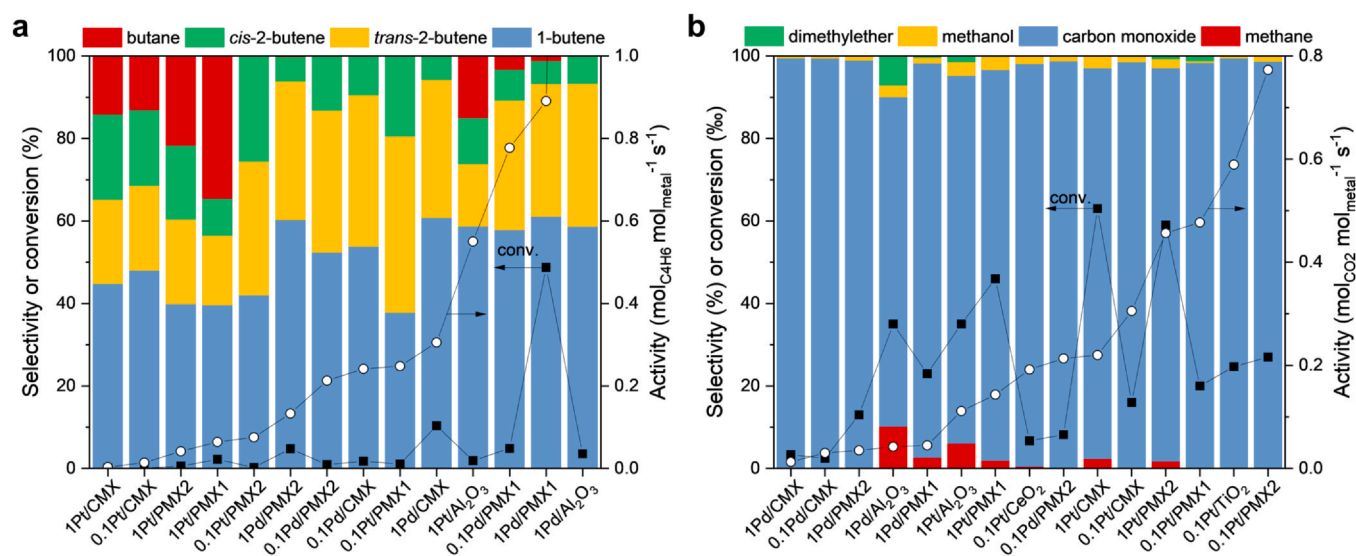


Fig. 6. Catalytic properties of unstacked catalysts. Catalytic performances (selectivity, conversion, molar activity) of all samples in butadiene hydrogenation (a) and CO_2 hydrogenation (b). In a, the Pt/ Al_2O_3 and Pd/ Al_2O_3 references were diluted in alumina at 10 wt% and 1 wt%, respectively. The activity of 1Pd/PMX1 is $4.5 s^{-1}$. Reaction conditions: $50^\circ C$, $H_2:C_4H_6:He = 10:2:88 mL/min$, 1 atm, 10 mg of catalyst drop casted on 50 mg of quartz wool. In b, the conversion unit is %. Reaction conditions: $275^\circ C$, $H_2:CO_2:Ar = 30:10:1.2 mL/min$, 3.1 MPa, 50 mg of catalyst intercalated with 350 mg of silica nanopowder.

high CO selectivity and yield at moderate temperature remains a challenge. Our metal/MXene catalysts were evaluated in gas-phase CO₂ hydrogenation at 3 MPa between 150 and 400 °C. For these tests involving a much higher amount of material than for butadiene hydrogenation (400 mg vs. 50 mg), quartz wool, which is difficult to handle and leads to an excessive catalyst bed volume, was substituted with silica nanopowder (Fig. 5d) as solid intercalant. The latter was found itself more efficient than titania and alumina (Fig. S15a). The samples were pretreated in H₂ flow for 1 h at 400 °C and atmospheric pressure. The noble metal-free unstacked MXenes appear poorly active, as shown in Fig. S15b. Like for butadiene hydrogenation, the activity order is: CMX < PMX2 < PMX1. This may be linked to the delamination degree evolving in the same order, which would lead to the highest number of surface active sites for PMX1 when unstacked with QW or silica.

The detailed results for the (unstacked) Pt and Pd-loaded MXenes are presented in Figs. S16–S17, while Fig. 6b summarizes the data at 275 °C. The main product is always CO, with more than 94 % selectivity. Methane, methanol and dimethylether were also detected in some cases – in maximal amount for alumina-supported references. The activity trends are reversed with respect to butadiene hydrogenation: for a given support, Pt catalysts are more active than Pd ones and for a given metal, PMX2 is more efficient than PMX1 and CMX. Consistently, Fig. S18 shows some anticorrelation between butadiene and CO₂ hydrogenation activities. Regarding the metal loading, though 0.1 wt% loaded catalysts are generally less active per gram of catalyst (i.e., conversions are lower) than 1 wt% loaded ones, they are always more active per mole of noble metal. Unlike Pd/Al₂O₃, most catalysts are relatively stable on heating and cooling (Fig. S16a,b), even Pd-based catalysts which conversely strongly deactivate during the hydrogenation of butadiene. The most efficient catalyst is the 0.1Pt/PMX2 SAC, with a CO selectivity of 99 % and an activity (turnover frequency) of 0.77 s⁻¹ at 275 °C [59,60]. Long-term testing of this sample at the same temperature (Fig. S19) showed that after an initial partial deactivation period, the catalyst kept a stable activity for two days.

Pt/TiO₂ and Pt/CeO₂ references loaded at 0.1 wt% Pt (STEM images in Fig. S10c,d) were evaluated in the same conditions. Compared to the MXene-supported SAC, Pt catalysts supported on TiO₂ (0.59 s⁻¹) and CeO₂ (0.19 s⁻¹) are less active, though these samples do not suffer from the possible limitation induced by MXene stacking. However, the similar (and best) performances of Pt/PMX2 and Pt/TiO₂ can be rationalized by the fact that PMX2 is, as previously discussed, the most oxidized and the most TiO₂-containing MXene. This suggests that TiO₂ may promote CO₂ adsorption on the composite or influence platinum activity via favorable metal-support interaction.

The CO₂ hydrogenation selectivity of MXene-supported catalysts depends on the promoting metal and the reaction conditions. With a PdRu/Ti₃C₂T_x catalyst, Bharat et al. reported a high selectivity to methanol in an aqueous phase containing ethylene glycol and NaBH₄ [31]. In contrast, working under atmospheric pressure and gas flow conditions, Ma et al. could change the selectivity of a Co/Ti₃C₂T_x catalyst from CO (86 % at 400 °C) to CH₄ (80 % at 400 °C) by N doping of the MXene [32]. Herein, by loading the MXenes with a low amount of Pt, we have shown that a CO selectivity close to 100 % can be reached at moderate temperature, with a high production rate.

More generally, this work shows that the gas-phase hydrogenation performances of MXene-based catalysts are sensitive to a number of interconnected parameters. Particularly, MXene delamination/unstacking and surface oxidation extents are key factors influencing reactant diffusion, metal-support interaction and surface reactivity.

4. Conclusions

Ti₃C₂T_x MXenes loaded with Pt or Pd (0.1–1 wt%) through wet impregnation of chloride salts were characterized by XRD, XPS, SEM and STEM, and were evaluated for gas-phase butadiene hydrogenation

and CO₂ hydrogenation in flow reactors. Starting from MXenes prepared using HF (CMX) or LiF-HCl (PMX) etching, the full procedure of sample conditioning for gas-phase catalytic testing was described, with step-by-step characterization. Using the LiF-HCl method, two samples were prepared, one of them (PMX2) being more defective and oxidized than the other (PMX1).

For CMX, which requires intercalation to delaminate in water, DMSO appears as the most efficient intercalant, and a relatively short sonication time (1 h) is preferred. In contrast, for PMX prepared in well-controlled conditions (PMX1), no additional intercalant is required and the delamination in water is much easier, if not spontaneous, which is a great advantage of the LiF-HCl method for MXene synthesis. It is shown that the delaminated MXenes can be easily decorated with ultra-dispersed metals and drop casted on (or intercalated with) oxide substrates such as silica. The latter process, which prevents the restacking of sheets and maximizes the reaction rates, is key to optimal catalytic testing in gas-phase reactions.

At low metal loading (0.1 wt%), Pt and Pd are dispersed as single atoms over the PMX surfaces, while clustering is observed on CMX, especially for Pd. Higher loadings, up to 1 wt%, favor nanoparticle formation, though a fraction of single atoms is still visible by STEM on Pt samples.

Systematic XPS analyses reveal that metal impregnation increases Ti oxidation along with amorphous carbon formation at the surface of MXenes. XRD supports MXene oxidation through the presence of anatase and rutile TiO₂ crystallites. In addition, Pt and Pd oxidation states are metal and support-dependent, but the average oxidation state overall increases with metal dispersion.

An anticorrelation between butadiene and CO₂ hydrogenation rates is observed: whereas Pd/PMX1 catalysts are overall more active for butadiene hydrogenation, Pt/PMX2 catalysts are more active for CO₂ hydrogenation. Notably, an unusual butadiene hydrogenation mechanism occurs on 0.1Pt/PMX SACs, which, compared to alumina-supported references and 1Pt/PMX nanocatalysts, exhibit higher selectivities to 2-butenes and no butane production. Remarkable performances are also obtained for CO₂ hydrogenation, namely CO₂ reduction to CO (RWGS reaction), in which the 0.1Pt/PMX SACs are selective at 98–99% and can reach a higher Pt-molar activity than any tested oxide-supported reference. It is likely that surface Ti oxidation plays a promoting role in this reaction.

In conclusion, beyond the fact that the LiF-HCl method is safer than the HF one to prepare Ti₃C₂T_x MXenes, this approach is also recommended to prepare heterogeneous catalysts for gas-phase reactions since it permits more efficient delamination. This both increases metal dispersion down to the single atom limit, and facilitates unstacking with solid substrates, leading to notable hydrogenation performances. Given the richness of the MXene family, the present work may serve as a guide to the preparation and evaluation of other MXene-based materials for thermal heterogeneous catalysis. In particular, from the knowledge on classical carbides, Mo and W-containing MXenes look promising as catalysts and catalyst supports for selective hydrogenation reactions.

Declaration of Competing Interest

The authors declare that they have no known competing financial interests or personal relationships that could have appeared to influence the work reported in this paper.

Acknowledgments

We thank R. Checa (CO₂ hydrogenation setup support), Y. Aizac (XRD), N. Bonnet & P. Mascunan (ICP & XRF), L. Burel (TEM), M. Bugnet (preliminary STEM observations), P. Chartier (Ti₃AlC₂ synthesis), and C. Molinet (Pt/CeO₂ reference sample preparation).

We acknowledge IRCATECH (ICP, XRF, XRD, XPS), CTμ (SEM), and CLYM (TEM & STEM) characterization platforms. We also thank China

Scholarship Council [Grant 202008330293] for YY's PhD funding, and ANR UltraCat [ANR-17-CE06-0008], ANR MXENECAT [ANR-18-CE08-014] & ICL MXCat programs for financial support. The IC2MP authors also acknowledge the financial support of the European Union (ERDF), Region Nouvelle Aquitaine and the French government's "Investissements d'Avenir" program (EUR INTREE, ANR-18-EURE-0010).

Appendix A. Supporting information

Supplementary data associated with this article can be found in the online version at [doi:10.1016/j.mtcata.2023.100010](https://doi.org/10.1016/j.mtcata.2023.100010).

References

- [1] M. Naguib, M. Kurtoglu, V. Presser, J. Lu, J. Niu, M. Heon, L. Hultman, Y. Gogotsi, M.W. Barsoum, Two-dimensional nanocrystals produced by exfoliation of Ti₃AlC₂, *Adv. Mater.* 23 (2011) 4248–4253, <https://doi.org/10.1002/adma.201102306>
- [2] B. Anasori, M.R. Lukatskaya, Y. Gogotsi, 2D metal carbides and nitrides (MXenes) for energy storage, *Nat. Rev. Mater.* 2 (2017) 1–17, <https://doi.org/10.1038/natrevmats.2016.98>
- [3] Á. Morales-García, F. Calle-Vallejo, F. Illas, MXenes: new horizons in catalysis, *ACS Catal.* 10 (2020) 13487–13503, <https://doi.org/10.1021/acscatal.0c03106>
- [4] A. VahidMohammadi, J. Rosen, Y. Gogotsi, The world of two-dimensional carbides and nitrides (MXenes), *Science* 372 (2021) eabf1581, <https://doi.org/10.1126/science.abf1581>
- [5] M. Alhabeib, K. Maleski, B. Anasori, P. Lelyukh, L. Clark, S. Sin, Y. Gogotsi, Guidelines for synthesis and processing of two-dimensional titanium carbide (Ti₃C₂Tx MXene), *Chem. Mater.* 29 (2017) 7633–7644, <https://doi.org/10.1021/acs.chemmater.7b02847>
- [6] X. Hui, X. Ge, R. Zhao, Z. Li, L. Yin, Interface chemistry on MXene-based materials for enhanced energy storage and conversion performance, *Adv. Funct. Mater.* 30 (2020) 2005190, <https://doi.org/10.1002/adfm.202005190>
- [7] M. Benchakar, L. Loupias, C. Garnero, T. Bilyk, C. Morais, C. Canaff, N. Guignard, S. Morisset, H. Pazniak, S. Hurand, P. Chartier, J. Pacaud, V. Mauchamp, M.W. Barsoum, A. Habrioux, S. Célérier, One MAX phase, different MXenes: a guideline to understand the crucial role of etching conditions on Ti₃C₂Tx surface chemistry, *Appl. Surf. Sci.* 530 (2020) 147209, <https://doi.org/10.1016/j.apsusc.2020.147209>
- [8] I.M. Chirica, A.G. Mirea, Ş. Neaţu, M. Florea, M.W. Barsoum, F. Neaţu, Applications of MAX phases and MXenes as catalysts, *J. Mater. Chem. A* 9 (2021) 19589–19612, <https://doi.org/10.1039/D1TA04097A>
- [9] P. Ranjan, V.B. Saptal, J.K. Bera, Recent advances in carbon dioxide adsorption, activation and hydrogenation to methanol using transition metal carbides, *ChemSusChem* 15 (2022) e202201183, <https://doi.org/10.1002/cssc.202201183>
- [10] M. Figueras, R.A. Gutiérrez, F. Viñes, P.J. Ramírez, J.A. Rodríguez, F. Illas, Supported molybdenum carbide nanoparticles as an excellent catalyst for CO₂ hydrogenation, *ACS Catal.* 11 (2021) 9679–9687, <https://doi.org/10.1021/acscatal.1c01738>
- [11] M. Abou Hamdan, A. Nassereddine, R. Checa, M. Jahjah, C. Pinel, L. Piccolo, N. Perret, Supported molybdenum carbide and nitride catalysts for carbon dioxide hydrogenation, *Front. Chem.* 8 (2020) 452, <https://doi.org/10.3389/fchem.2020.00452>
- [12] Á. Morales-García, A. Fernández-Fernández, F. Viñes, F. Illas, CO₂ abatement using two-dimensional MXene carbides, *J. Mater. Chem. A* 6 (2018) 3381–3385, <https://doi.org/10.1039/C7TA11379J>
- [13] M. López, Á. Morales-García, F. Viñes, F. Illas, Thermodynamics and kinetics of molecular hydrogen adsorption and dissociation on MXenes: relevance to heterogeneously catalyzed hydrogenation reactions, *ACS Catal.* 11 (2021) 12850–12857, <https://doi.org/10.1021/acscatal.1c03150>
- [14] I. Persson, J. Halim, H. Lind, T.W. Hansen, J.B. Wagner, L.-Å. Näslund, V. Darakchieva, J. Palisaitis, J. Rosen, P.O.Å. Persson, 2D transition metal carbides (MXenes) for carbon capture, *Adv. Mater.* 31 (2019) 1805472, <https://doi.org/10.1002/adma.201805472>
- [15] Y. Chen, C. Liu, S. Guo, T. Mu, L. Wei, Y. Lu, CO₂ capture and conversion to value-added products promoted by MXene-based materials, *Green Energy Environ.* 7 (2022) 394–410, <https://doi.org/10.1016/j.gjee.2020.11.008>
- [16] R. Morales-Salvador, J.D. Gouveia, Á. Morales-García, F. Viñes, J.R.B. Gomes, F. Illas, Carbon capture and usage by MXenes, *ACS Catal.* 11 (2021) 11248–11255, <https://doi.org/10.1021/acscatal.1c02663>
- [17] H. Zhou, Z. Chen, E. Kountoupi, A. Tsoukalou, P.M. Abdala, P. Florian, A. Fedorov, C.R. Müller, Two-dimensional molybdenum carbide 2D-Mo₂C as a superior catalyst for CO₂ hydrogenation, *Nat. Commun.* 12 (2021) 5510, <https://doi.org/10.1038/s41467-021-25784-0>
- [18] Z. Li, N.H. Attanayake, J.L. Blackburn, E.M. Miller, Carbon dioxide and nitrogen reduction reactions using 2D transition metal dichalcogenide (TMDC) and carbide/nitride (MXene) catalysts, *Energy Environ. Sci.* 14 (2021) 6242–6286, <https://doi.org/10.1039/D1EE03211A>
- [19] N.H. Attanayake, H.R. Banjade, A.C. Thenuwara, B. Anasori, Q. Yan, D.R. Strongin, Electrocatalytic CO₂ reduction on earth abundant 2D Mo₂C and Ti₃C₂ MXenes, *Chem. Commun.* 57 (2021) 1675–1678, <https://doi.org/10.1039/DOCC05822J>
- [20] J. Diao, M. Hu, Z. Lian, Z. Li, H. Zhang, F. Huang, B. Li, X. Wang, D.S. Su, H. Liu, Ti₃C₂Tx MXene catalyzed ethylbenzene dehydrogenation: active sites and mechanism exploration from both experimental and theoretical aspects, *ACS Catal.* 8 (2018) 10051–10057, <https://doi.org/10.1021/acscatal.8b02002>
- [21] M. Naguib, W. Tang, K.L. Browning, G.M. Veith, V. Maliekkal, M. Neurock, A. Villa, Catalytic activity of Ti-based MXenes for the hydrogenation of furfural, *ChemCatChem* 12 (2020) 5733–5742, <https://doi.org/10.1002/cctc.202000977>
- [22] E. Blanco, A. Rosenkranz, R. Espinoza-González, V.M. Fuenzalida, Z. Zhang, S. Suárez, N. Escalona, Catalytic performance of 2D-Mxene nano-sheets for the hydrodeoxygenation (HDO) of lignin-derived model compounds, *Catal. Commun.* 133 (2020) 105833, <https://doi.org/10.1016/j.catcom.2019.105833>
- [23] T. Hou, Q. Luo, Q. Li, H. Zu, P. Cui, S. Chen, Y. Lin, J. Chen, X. Zheng, W. Zhu, S. Liang, J. Yang, L. Wang, Modulating oxygen coverage of Ti₃C₂Tx MXenes to boost catalytic activity for HCOOH dehydrogenation, *Nat. Commun.* 11 (2020) 4251, <https://doi.org/10.1038/s41467-020-18091-7>
- [24] R. Thakur, M. Hoffman, A. VahidMohammadi, J. Smith, M. Chi, B. Tatarchuk, M. Beidaghi, C.A. Carrero, Multilayered two-dimensional V₂CT_x MXene for methane dehydroaromatization, *ChemCatChem* 12 (2020) 3639–3643, <https://doi.org/10.1002/cctc.201902366>
- [25] R. Thakur, A. VahidMohammadi, J. Smith, M. Hoffman, J. Moncada, M. Beidaghi, C.A. Carrero, Insights into the genesis of a selective and coke-resistant MXene-based catalyst for the dry reforming of methane, *ACS Catal.* 10 (2020) 5124–5134, <https://doi.org/10.1021/acscatal.0c00797>
- [26] E.B. Deeva, A. Kurlov, P.M. Abdala, D. Lebedev, S.M. Kim, C.P. Gordon, A. Tsoukalou, A. Fedorov, C.R. Müller, In situ XANES/XRD study of the structural stability of two-dimensional molybdenum carbide Mo₂CTx: implications for the catalytic activity in the water–gas shift reaction, *Chem. Mater.* 31 (2019) 4505–4513, <https://doi.org/10.1021/acs.chemmater.9b01105>
- [27] Z. Li, L. Yu, C. Milligan, T. Ma, L. Zhou, Y. Cui, Z. Qi, N. Libretto, B. Xu, J. Luo, E. Shi, Z. Wu, H. Xin, W.N. Delgass, J.T. Miller, Y. Wu, Two-dimensional transition metal carbides as supports for tuning the chemistry of catalytic nanoparticles, *Nat. Commun.* 9 (2018) 5258, <https://doi.org/10.1038/s41467-018-07502-5>
- [28] C. Yang, Q. Jiang, W. Li, H. He, L. Yang, Z. Lu, H. Huang, Ultrafine Pt nanoparticle-decorated 3D hybrid architectures built from reduced graphene oxide and MXene nanosheets for methanol oxidation, *Chem. Mater.* 31 (2019) 9277–9287, <https://doi.org/10.1021/acs.chemmater.9b02115>
- [29] L. Liu, Q. Zhao, R. Liu, L. Zhu, Hydrogen adsorption-induced catalytic enhancement over Cu nanoparticles immobilized by layered Ti₃C₂ MXene, *Appl. Catal. B Environ.* 252 (2019) 198–204, <https://doi.org/10.1016/j.apcatb.2019.04.026>
- [30] Q. Chen, W. Jiang, G. Fan, Pt nanoparticles on Ti₃C₂Tx-based MXenes as efficient catalysts for the selective hydrogenation of nitroaromatic compounds to amines, *Dalton Trans.* 49 (2020) 14914–14920, <https://doi.org/10.1039/D0DT02594A>
- [31] G. Bharath, K. Rambabu, A. Hai, I. Othman, N. Ponpandian, F. Banat, P. Loke Show, Hybrid Pd50-Ru50/MXene (Ti₃C₂Tx) nanocatalyst for effective hydrogenation of CO₂ to methanol toward climate change control, *Chem. Eng. J.* 414 (2021) 128869, <https://doi.org/10.1016/j.cej.2021.128869>
- [32] J. Ma, Q. Jiang, Y. Zhou, W. Chu, S. Perathoner, C. Jiang, K.-H. Wu, G. Centi, Y. Liu, Tuning the chemical properties of Co–Ti₃C₂Tx MXene materials for catalytic CO₂ reduction, *Small* 17 (2021) 2007509, <https://doi.org/10.1002/sml.202007509>
- [33] M. Bat-Erdene, M. Batmunkh, B. Sainbileg, M. Hayashi, A.S.R. Bati, J. Qin, H. Zhao, Y.L. Zhong, J.G. Shapter, Highly dispersed Ru nanoparticles on boron-doped Ti₃C₂Tx (MXene) nanosheets for synergistic enhancement of electrocatalytic hydrogen evolution, *Small* 17 (2021) 2102218, <https://doi.org/10.1002/sml.202102218>
- [34] Z. Li, Y. Xiao, P.R. Chowdhury, Z. Wu, T. Ma, J.Z. Chen, G. Wan, T.-H. Kim, D. Jing, P. He, P.J. Potdar, L. Zhou, Z. Zeng, X. Ruan, J.T. Miller, J.P. Greeley, Y. Wu, A. Varma, Direct methane activation by atomically thin platinum nanolayers on two-dimensional metal carbides, *Nat. Catal.* 4 (2021) 882–891, <https://doi.org/10.1038/s41929-021-00686-y>
- [35] A. Wang, J. Li, T. Zhang, Heterogeneous single-atom catalysis, *Nat. Rev. Chem.* 2 (2018) 65–81, <https://doi.org/10.1038/s41570-018-0010-1>
- [36] S. Mitchell, J. Pérez-Ramírez, Atomically precise control in the design of low-nuclearity supported metal catalysts, *Nat. Rev. Mater.* (2021) 1–17, <https://doi.org/10.1038/s41578-021-00360-6>
- [37] L. Piccolo, Restructuring effects of the chemical environment in metal nanocatalysis and single-atom catalysis, *Catal. Today* 373 (2021) 80–97, <https://doi.org/10.1016/j.cattod.2020.03.052>
- [38] P. Serp, D. Pham Minh (Eds.), Supported Metal Single Atom Catalysis, Wiley-VCH, Weinheim, 2022. <https://doi.org/10.1002/9783527830169>
- [39] D. Zhao, Z. Chen, W. Yang, S. Liu, X. Zhang, Y. Yu, W.-C. Cheong, L. Zheng, F. Ren, G. Ying, X. Cao, D. Wang, Q. Peng, G. Wang, C. Chen, MXene (Ti₃C₂) vacancy-confined single-atom catalyst for efficient functionalization of CO₂, *J. Am. Chem. Soc.* 141 (2019) 4086–4093, <https://doi.org/10.1021/jacs.8b13579>
- [40] V. Ramalingam, P. Varadhan, H.-C. Fu, H. Kim, D. Zhang, S. Chen, L. Song, D. Ma, Y. Wang, H.N. Alshareef, J.-H. He, Heteroatom-mediated interactions between ruthenium single atoms and an MXene support for efficient hydrogen evolution, *Adv. Mater.* 31 (2019) 1903841, <https://doi.org/10.1002/adma.201903841>
- [41] J. Gu, Q. Zhu, Y. Shi, H. Chen, D. Zhang, Z. Du, S. Yang, Single zinc atoms immobilized on MXene (Ti₃C₂Clx) layers toward dendrite-free lithium metal anodes, *ACS Nano* 14 (2020) 891–898, <https://doi.org/10.1021/acsnano.9b08141>
- [42] S. Zhao, Y. Wen, X. Peng, Y. Mi, X. Liu, Y. Liu, L. Zhuo, G. Hu, J. Luo, X. Tang, Isolated single-atom Pt sites for highly selective electrocatalytic hydrogenation of formaldehyde to methanol, *J. Mater. Chem. A* 8 (2020) 8913–8919, <https://doi.org/10.1039/D0TA00190B>
- [43] Q. Zhao, C. Zhang, R. Hu, Z. Du, J. Gu, Y. Cui, X. Chen, W. Xu, Z. Cheng, S. Li, B. Li, Y. Liu, W. Chen, C. Liu, J. Shang, L. Song, S. Yang, Selective etching quaternary

- MAX phase toward single atom copper immobilized MXene (Ti3C2Clx) for efficient CO₂ electroreduction to methanol, *ACS Nano* 15 (2021) 4927–4936, <https://doi.org/10.1021/acsnano.0c09755>
- [44] S. Zhou, Y. Zhao, R. Shi, Y. Wang, A. Ashok, F. Héraly, T. Zhang, J. Yuan, Vacancy-rich MXene-immobilized Ni single atoms as a high-performance electrocatalyst for the hydrazine oxidation reaction, *Adv. Mater.* 34 (2022) 2204388, <https://doi.org/10.1002/adma.202204388>
- [45] X. Guo, H. Gao, S. Wang, G. Yang, X. Zhang, J. Zhang, H. Liu, G. Wang, MXene-based aerogel anchored with antimony single atoms and quantum dots for high-performance potassium-ion batteries, *Nano Lett.* 22 (2022) 1225–1232, <https://doi.org/10.1021/acs.nanolett.1c04389>
- [46] D.A. Kuznetsov, Z. Chen, P.V. Kumar, A. Tsoukalou, A. Kierzkowska, P.M. Abdala, O.V. Safonova, A. Fedorov, C.R. Müller, Single site cobalt substitution in 2D molybdenum carbide (MXene) enhances catalytic activity in the hydrogen evolution reaction, *J. Am. Chem. Soc.* 141 (2019) 17809–17816, <https://doi.org/10.1021/jacs.9b08897>
- [47] W. Peng, M. Luo, X. Xu, K. Jiang, M. Peng, D. Chen, T.-S. Chan, Y. Tan, Spontaneous atomic ruthenium doping in Mo2CTx MXene defects enhances electrocatalytic activity for the nitrogen reduction reaction, *Adv. Energy Mater.* 10 (2020) 2001364, <https://doi.org/10.1002/aenm.202001364>
- [48] D.A. Kuznetsov, Z. Chen, P.M. Abdala, O.V. Safonova, A. Fedorov, C.R. Müller, Single-atom-substituted Mo2CTx:Fe-layered carbide for selective oxygen reduction to hydrogen peroxide: tracking the evolution of the MXene phase, *J. Am. Chem. Soc.* 143 (2021) 5771–5778, <https://doi.org/10.1021/jacs.1c00504>
- [49] H. Zhou, Z. Chen, A.V. López, E.D. López, E. Lam, A. Tsoukalou, E. Willinger, D.A. Kuznetsov, D. Mance, A. Kierzkowska, F. Donat, P.M. Abdala, A. Comas-Vives, C. Copéret, A. Fedorov, C.R. Müller, Engineering the Cu/Mo2CTx (MXene) interface to drive CO₂ hydrogenation to methanol, *Nat. Catal.* 4 (2021) 860–871, <https://doi.org/10.1038/s41929-021-00684-0>
- [50] J. Zhang, Y. Zhao, X. Guo, C. Chen, C.-L. Dong, R.-S. Liu, C.-P. Han, Y. Li, Y. Gogotsi, G. Wang, Single platinum atoms immobilized on an MXene as an efficient catalyst for the hydrogen evolution reaction, *Nat. Catal.* 1 (2018) 985, <https://doi.org/10.1038/s41929-018-0195-1>
- [51] S. Park, Y.-L. Lee, Y. Yoon, S.Y. Park, S. Yim, W. Song, S. Myung, K.-S. Lee, H. Chang, S.S. Lee, K.-S. An, Reducing the high hydrogen binding strength of vanadium carbide MXene with atomic Pt confinement for high activity toward HER, *Appl. Catal. B Environ.* 304 (2022) 120989, <https://doi.org/10.1016/j.apcatb.2021.120989>
- [52] H. Gu, X. Li, J. Zhang, W. Chen, Theoretical predictions, experimental modulation strategies, and applications of MXene-supported atomically dispersed metal sites, *Small* 18 (2022) 2105883, <https://doi.org/10.1002/smll.202105883>
- [53] Q. Zhu, Y. Cui, Y. Zhang, Z. Cao, Y. Shi, J. Gu, Z. Du, B. Li, S. Yang, Strategies for engineering the MXenes toward highly active catalysts, *Mater. Today Nano* 13 (2021) 100104, <https://doi.org/10.1016/j.mtnano.2020.100104>
- [54] R. Wang, M. Li, K. Sun, Y. Zhang, J. Li, W. Bao, Element-doped MXenes: mechanism, synthesis, and applications, *Small* 18 (2022) 2201740, <https://doi.org/10.1002/smll.202201740>
- [55] M. Keyhanian, D. Farmanzadeh, Á. Morales-García, F. Illas, Effect of oxygen termination on the interaction of first row transition metals with M2C MXenes and the feasibility of single-atom catalysts, *J. Mater. Chem. A* 10 (2022) 8846–8855, <https://doi.org/10.1039/D1TA10252D>
- [56] C. Louis, L. Delannoy, Chapter one – selective hydrogenation of polyunsaturated hydrocarbons and unsaturated aldehydes over bimetallic catalysts, *Adv. Catal. Academic Press*, 2019, pp. 1–88, <https://doi.org/10.1016/bs.acat.2019.08.002>
- [57] S. Liu, S. Tan, B. Bian, H. Yu, Q. Wu, Z. Liu, F. Yu, L. Li, S. Yu, X. Song, Z. Song, Isobutane/2-butene alkylation catalyzed by Brønsted–Lewis acidic ionic liquids, *RSC Adv.* 8 (2018) 19551–19559, <https://doi.org/10.1039/C8RA03485K>
- [58] Q. Wang, X. Zheng, J. Wu, Y. Wang, D. Wang, Y. Li, Recent progress in thermal conversion of CO₂ via single-atom site catalysis, *Small Struct.* 3 (2022) 2200059, <https://doi.org/10.1002/sstr.202200059>
- [59] Y.A. Daza, J.N. Kuhn, CO₂ conversion by reverse water gas shift catalysis: comparison of catalysts, mechanisms and their consequences for CO₂ conversion to liquid fuels, *RSC Adv.* 6 (2016) 49675–49691, <https://doi.org/10.1039/C6RA05414E>
- [60] A.M. Bahmanpour, M. Signorile, O. Kröcher, Recent progress in syngas production via catalytic CO₂ hydrogenation reaction, *Appl. Catal. B Environ.* 295 (2021) 120319, <https://doi.org/10.1016/j.apcatb.2021.120319>
- [61] X. Wang, C. Garnero, G. Rocharod, D. Magne, S. Morisset, S. Hurand, P. Chartier, J. Rousseau, T. Cabioch, C. Coutanceau, V. Mauchamp, V. Mauchamp, A new etching environment (FeF₃/HCl) for the synthesis of two-dimensional titanium carbide MXenes: a route towards selective reactivity vs. water, *J. Mater. Chem. A* 5 (2017) 22012–22023, <https://doi.org/10.1039/C7TA01082F>
- [62] J.P. Brunelle, Preparation of catalysts by metallic complex adsorption on mineral oxides, *Pure Appl. Chem.* 50 (1978) 1211–1229, <https://doi.org/10.1351/pac19780091211>
- [63] K. Ding, G. Yang, HCl-assisted pyrolysis of PdCl₂ to immobilize palladium nanoparticles on multi-walled carbon nanotubes, *Mater. Chem. Phys.* 123 (2010) 498–501, <https://doi.org/10.1016/j.matchemphys.2010.05.003>
- [64] M.R. Lukatskaya, O. Mashtalir, C.E. Ren, Y. Dall'Agnes, P. Rozier, P.L. Taberna, M. Naguib, P. Simon, M.W. Barsoum, Y. Gogotsi, Cation intercalation and high volumetric capacitance of two-dimensional titanium carbide, *Science* 341 (2013) 1502–1505, <https://doi.org/10.1126/science.1241488>
- [65] J. Yan, C.E. Ren, K. Maleski, C.B. Hatter, B. Anasori, P. Urbankowski, A. Sarycheva, Y. Gogotsi, Flexible MXene/graphene films for ultrafast supercapacitors with outstanding volumetric capacitance, *Adv. Funct. Mater.* 27 (2017) 1701264, <https://doi.org/10.1002/adfm.201701264>
- [66] M.A. Hope, A.C. Forse, K.J. Griffith, M.R. Lukatskaya, M. Ghidui, Y. Gogotsi, C.P. Grey, NMR reveals the surface functionalisation of Ti3C2 MXene, *Phys. Chem. Chem. Phys.* 18 (2016) 5099–5102, <https://doi.org/10.1039/C6CP00330C>
- [67] C.J. Zhang, S. Pinilla, N. McEvoy, C.P. Cullen, B. Anasori, E. Long, S.-H. Park, A. Seral-Ascaso, A. Shmeliov, D. Krishnan, C. Morant, X. Liu, G.S. Duesberg, Y. Gogotsi, V. Nicolosi, Oxidation stability of colloidal two-dimensional titanium carbides (MXenes), *Chem. Mater.* 29 (2017) 4848–4856, <https://doi.org/10.1021/acs.chemmater.7b00745>
- [68] S. Huang, V.N. Mochalin, Hydrolysis of 2D transition-metal carbides (MXenes) in colloidal solutions, *Inorg. Chem.* 58 (2019) 1958–1966, <https://doi.org/10.1021/acs.inorgchem.8b02890>
- [69] V. Natu, M. Benchakar, C. Canaff, A. Habrioux, S. Célériér, M.W. Barsoum, A critical analysis of the X-ray photoelectron spectra of Ti3C2Tx MXenes, *Matter* 4 (2021) 1224–1251, <https://doi.org/10.1016/j.matt.2021.01.015>
- [70] J. Halim, K.M. Cook, M. Naguib, P. Eklund, Y. Gogotsi, J. Rosen, M.W. Barsoum, X-ray photoelectron spectroscopy of select multi-layered transition metal carbides (MXenes), *Appl. Surf. Sci.* 362 (2016) 406–417, <https://doi.org/10.1016/j.apsusc.2015.11.089>
- [71] I. Persson, L.-Å. Näslund, J. Halim, M.W. Barsoum, V. Darakchieva, J. Palisaitis, J. Rosen, P.O.Å. Persson, On the organization and thermal behavior of functional groups on Ti3C2 MXene surfaces in vacuum, *2D Mater.* 5 (2018) 015002, <https://doi.org/10.1088/2053-1583/aa89cd>
- [72] T. Schultz, N.C. Frey, K. Hantanasirisakul, S. Park, S.J. May, V.B. Shenoy, Y. Gogotsi, N. Koch, Surface termination dependent work function and electronic properties of Ti3C2Tx MXene, *Chem. Mater.* 31 (2019) 6590–6597, <https://doi.org/10.1021/acs.chemmater.9b00414>
- [73] L.-Å. Näslund, I. Persson, XPS spectra curve fittings of Ti3C2Tx based on first principles thinking, *Appl. Surf. Sci.* 593 (2022) 153442, <https://doi.org/10.1016/j.apsusc.2022.153442>
- [74] M. Paulis, H. Peyrard, M. Montes, Influence of chlorine on the activity and stability of Pt/Al₂O₃ catalysts in the complete oxidation of toluene, *J. Catal.* 199 (2001) 30–40, <https://doi.org/10.1006/jcat.2000.3146>
- [75] M. Ghidui, J. Halim, S. Kota, D. Bish, Y. Gogotsi, M.W. Barsoum, Ion-exchange and cation solvation reactions in Ti3C2 MXene, *Chem. Mater.* 28 (2016) 3507–3514, <https://doi.org/10.1021/acs.chemmater.6b01275>
- [76] O. Mashtalir, K.M. Cook, V.N. Mochalin, M. Crowe, M.W. Barsoum, Y. Gogotsi, Dye adsorption and decomposition on two-dimensional titanium carbide in aqueous media, *J. Mater. Chem. A* 2 (2014) 14334–14338, <https://doi.org/10.1039/C4TA02638A>
- [77] S. Célériér, S. Hurand, C. Garnero, S. Morisset, M. Benchakar, A. Habrioux, P. Chartier, V. Mauchamp, N. Findling, B. Larson, E. Ferrage, Hydration of Ti3C2Tx MXene: an interstratification process with major implications on physical properties, *Chem. Mater.* 31 (2019) 454–461, <https://doi.org/10.1021/acs.chemmater.8b03976>
- [78] M. Wojnicki, R.P. Socha, Z. Pędzich, K. Mech, T. Tokarski, K. Fitzner, Palladium(II) chloride complex ion recovery from aqueous solutions using adsorption on activated carbon, *J. Chem. Eng. Data* 63 (2018) 702–711, <https://doi.org/10.1021/acs.jced.7b00885>
- [79] A. Shahzad, K. Rasool, W. Miran, M. Nawaz, J. Jang, K.A. Mahmoud, D.S. Lee, Two-dimensional Ti3C2Tx MXene nanosheets for efficient copper removal from water, *ACS Sustain. Chem. Eng.* 5 (2017) 11481–11488, <https://doi.org/10.1021/acssuschemeng.7b02695>
- [80] A. Kurlov, E.B. Deeva, P.M. Abdala, D. Lebedev, A. Tsoukalou, A. Comas-Vives, A. Fedorov, C.R. Müller, Exploiting two-dimensional morphology of molybdenum oxycarbide to enable efficient catalytic dry reforming of methane, *Nat. Commun.* 11 (2020) 4920, <https://doi.org/10.1038/s41467-020-18721-0>
- [81] X. Zhao, A. Vashisth, E. Prehn, W. Sun, S.A. Shah, T. Habib, Y. Chen, Z. Tan, J.L. Lutkenhaus, M. Radovic, M.J. Green, Antioxidants unlock shelf-stable Ti3C2Tx (MXene) nanosheet dispersions, *Matter* 1 (2019) 513–526, <https://doi.org/10.1016/j.matt.2019.05.020>
- [82] A. Limcharoen, C. Pakpum, P. Lisuwan, An X-ray photoelectron spectroscopy investigation of redeposition from fluorine-based plasma etch on magnetic recording slider head substrate, *Procedia Eng.* 32 (2012) 1043–1049, <https://doi.org/10.1016/j.proeng.2012.02.052>
- [83] Z. Zhang, S.H. Lim, D.M.Y. Lai, S.Y. Tan, X.Q. Koh, J. Chai, S.J. Wang, H. Jin, J.S. Pan, Probing the oxidation behavior of Ti2AlC MAX phase powders between 200 and 1000 °C, *J. Eur. Ceram. Soc.* 37 (2017) 43–51, <https://doi.org/10.1016/j.jeurceramsoc.2016.08.004>
- [84] G.C. Bond, G. Webb, P.B. Wells, J.M. Winterbottom, The hydrogenation of alka-dienes. Part I. The hydrogenation of buta-1,3-diene catalysed by the noble group VIII metals, *J. Chem. Soc.* (1965) 3218–3227, <https://doi.org/10.1039/JR9650003218>
- [85] J.P. Boitiaux, J. Cosyns, E. Robert, Hydrogenation of unsaturated hydrocarbons in liquid phase on palladium, platinum and rhodium catalysts, *Appl. Catal.* 35 (1987) 193–209, [https://doi.org/10.1016/S0166-9834\(00\)82860-2](https://doi.org/10.1016/S0166-9834(00)82860-2)
- [86] R.B. Moyes, P.B. Wells, J. Grant, N.Y. Salman, Electronic effects in butadiene hydrogenation catalysed by the transition metals, *Appl. Catal. A Gen.* 229 (2002) 251–259, [https://doi.org/10.1016/S0926-860X\(02\)00033-9](https://doi.org/10.1016/S0926-860X(02)00033-9)

- [87] M. Primet, M. El Azhar, M. Guenin, Influence of the support towards platinum catalysed 1,3-butadiene hydrogenation, *Appl. Catal.* 58 (1990) 241–253, [https://doi.org/10.1016/S0166-9834\(00\)82293-9](https://doi.org/10.1016/S0166-9834(00)82293-9)
- [88] Y. Cao, Q. Deng, Z. Liu, D. Shen, T. Wang, Q. Huang, S. Du, N. Jiang, C.-T. Lin, J. Yu, Enhanced thermal properties of poly(vinylidene fluoride) composites with ultrathin nanosheets of MXene, *RSC Adv.* 7 (2017) 20494–20501, <https://doi.org/10.1039/C7RA00184C>
- [89] J.C. Yu, J. Yu, W. Ho, Z. Jiang, L. Zhang, Effects of F-doping on the photocatalytic activity and microstructures of nanocrystalline TiO₂ powders, *Chem. Mater.* 14 (2002) 3808–3816, <https://doi.org/10.1021/cm020027c>
- [90] T. Len, M. Bahri, O. Ersen, Y. Lefkir, L. Cardenas, I.J. Villar-Garcia, V.P. Dieste, J. Llorca, N. Perret, R. Checa, E. Puzenat, P. Afanasiev, F. Morfin, L. Piccolo, Ultradispersed Mo/TiO₂ catalysts for CO₂ hydrogenation to methanol, *Green Chem.* 23 (2021) 7259–7268, <https://doi.org/10.1039/D1GC01761F>